VIII. RADIO ASTRONOMY

Academic and Research Staff

Prof. Alan H. Barrett
Prof. Bernard F. Burke
Prof. R. Marcus Price
Prof. David H. Staelin
Dr. Philip C. Myers
Dr. Alan Parrish
Dr. Philip W. Rosenkranz
John W. Barrett
D. Cosmo Papa

Graduate Students

Patrick C. Crane
Arthur D. Fisher
Thomas S. Giuffrida
Aubrey D. Haschick
Paul T. Ho
Kai-Shue Lam
William H. Ledsham
Sylvester Lee
Kwok-Yung Lo
Robert N. Martin
Robert J. Parr
Ronald L. Pettyjohn
Bruce M. Schechter
Matthew H. Schneps
Gary K. Stimac
Robert C. Walker

RESEARCH OBJECTIVES AND SUMMARY OF RESEARCH

JSEP

1. Microwave Propagation in the Terrestrial Atmosphere

Joint Services Electronics Program (Contract DAAB07-74-C-0630)

Alan H. Barrett

For some time there has been a discrepancy between theoretical and experimental values of microwave absorption in the terrestrial atmosphere. We felt that this is due to shortcomings in the theoretical treatment of pressure broadening when the significant overlap between adjacent lines occurs. Formal theories of pressure broadening have been given but have not been applied to the specific case of microwave energy transfer in the atmosphere where self-broadening and foreign gas broadening of O_2 and H_2O over the temperature and pressure range of the atmosphere must be included. We have adapted the theory for O_2-O_2 and O_2-N_2 collisions. We have found significant departures from results with previous simpler theory. In particular, we now note less absorption ($\approx$15%) in the wings of the lines, and more ($\approx$8%) in the centers of the lines, which gives better agreement with experimental results. The computations are being extended to include all O_2 lines of importance and microwave and infrared lines of H_2O. Details of this work are reported in Section VIII-A.

JSEP

2. Microwave Spectroscopy of the Interstellar Medium

National Science Foundation (Grants GP-40484X and MPS73-05042-A01)

Alan H. Barrett

In radio spectroscopic studies of dark interstellar clouds we have concentrated on three specific areas: correlation of extinction by dust with molecular H_2CO, OH, and atomic hydrogen; kinematic and physical conditions of these clouds as determined by radio observation of CO, CS, NH_3, CN, OCS, SO, SiO, and CH_3OH; and electron properties of these clouds by observation of the continuum emission and recombination lines.

Two specific molecular sources are receiving detailed attention. Orion A is being mapped in six NH_3 lines and the IR source in Orion is being studied in five transitions

in CH_3OH. Maps of Sgr B2 will be made in the CN, OCS, SO, CS, SiO, and CH_3OH lines.

3. Noninvasive Sensing of Subcutaneous Temperatures Using Microwave Thermography

National Institutes of Health (Grant 1 RO1 GM20370-02)

Alan H. Barrett

Our program to evaluate the capability of microwave radiometers to sense subcutaneous temperatures for medical diagnostic purposes has reached the clinical evaluation stage. A radiometer operating at 3.3 GHz has been packaged for hospital use and is now in routine operation at Faulkner Hospital, in Boston. The initial clinical application is the detection of subsurface temperature anomalies associated with tumors of the breast. Microwave examinations are made in conjunction with the physician's clinical examination, infrared thermography, mammography, and a biopsy examination. Conclusions about the usefulness of microwave thermography must await the study of many more patients.

A radiometer operating at 1.3 GHz is undergoing laboratory development and test and will be used in the laboratory to check our experimental technique.

4. Experiments for Microwave Temperature Sounding of the Mesosphere and Upper Stratosphere

National Aeronautics and Space Administration (Contract NAS1-10693)

Philip W. Rosenkranz, David H. Staelin

The extremely opaque O_2 resonances near 60 GHz provide the opportunity for satellite-borne microwave radiometers to measure thermal radiation originating from levels up to 75 km altitude. It appears to be possible on a global scale to map the atmospheric temperature profile from 0-75 km altitude with ~5-20 km vertical resolution and 100-400 km horizontal resolution.

A previously discovered discrepancy between theory and the observed 23_-, 25_-, 27_-, 29_-, and 31_- resonances of O_2 may be partially explained by a recent improvement in theoretical expressions for O_2 absorption at these frequencies. This is discussed in Section VIII-B.

Further measurements are planned to refine the atmospheric absorption coefficients. A final proposal for a space flight experiment will also be prepared during the coming year.

5. Environmental Sensing with Nimbus Satellite Passive Microwave Spectrometers

National Aeronautics and Space Administration (Contract NAS5-21980 and NAS5-20091)

D. H. Staelin, Klaus F. Kunzi, Philip W. Rosenkranz

The Nimbus-5 Earth observatory satellite was launched in December, 1972 into a nearly circular polar orbit at 592 NM altitude. The 5-channel microwave spectrometer

(NEMS) views the nadir with half-power 10° beamwidth. Individual channels are located at a weak water-vapor resonance, in a spectral window, and at 3 positions on the edge of the oxygen absorption band; the center frequencies are 22.235, 31.4, 53.65, 54.9, and 58.8 GHz.

Manuscripts have been prepared for publication which summarize the performance of NEMS in measurements of atmospheric temperature profiles, atmospheric water vapor and liquid water content over ocean, water-vapor and temperature profiles in the presence of clouds, and snow and ice properties. Improvements are being made in the characterization of the physical processes involved and in the techniques for estimation of the desired geophysical parameters.

The Nimbus-6 satellite, which will be launched in 1975, will carry a scanned version of NEMS, and provide two complete global maps with 200-km resolution each day. Preparations for this experiment are under way.

JSEP

A. CALCULATION OF PRESSURE-BROADENING EFFECTS IN OXYGEN MICROWAVE ABSORPTION

Joint Services Electronics Program (Contract DAAB07-74-C-0630)
U.S. Air Force – Electronic Systems Division (Contract F19628-73-C-0196)

Alan H. Barrett, Kai S. Lam

1. Introduction

The interpretation of data from atmospheric microwave sensing experiments requires detailed knowledge of microwave absorption by molecular oxygen. In particular, we require a theory capable of calculating widths for collision-broadened lines and accounting for line-overlapping effects. This problem has long received widespread attention. Among the more recent workers were Van Vleck and Weisskopf[1] and Gross,[2] who treated the absorber as a classical harmonic oscillator. Anderson[3] introduced the first complete semiquantum-mechanical procedure to compute the linewidth of a resolved line. Baranger[4] introduced a formal quantum-mechanical theory for overlapping lines and initiated the line-space concept. Later, Fano[5] and Ben-Reuven[6] developed the Liouville (line) space formalism further and made elaborate use of quantum-statistical methods to treat pressure broadening as a relaxation process and Gordon[7] introduced a semiclassical theory of pressure broadening based on the reorientation of molecules during collision. Gersten and Foley[8] and Dillon and his co-workers[9] adopted the Fano formalism and developed it to a computable state for the case of oxygen. The most recent many-body formulation of the pressure-broadening problem is that of Ross[10] and Bezzerides[11] but this formulation is still unsuitable for specific applications.

In our present calculations we attempt to treat atmospheric oxygen microwave absorption, in which the main agents of line broadening are oxygen and nitrogen. Numerical results have been obtained only for oxygen-oxygen interaction and for lines arising from rotation quantum number N = 1 through 11 for T = 300°K. (At ordinary atmospheric temperatures, lines from N = 1 through ~33 should be included.) The inclusion of more lines and the N_2-O_2 interaction would present no new features in the computation procedure; the only changes would be the appearance of a larger matrix and alterations of numerical values for the parameters of intermolecular potential. These features will be included in a future computation.

We adopt essentially the Dillon approach, which is the foreign gas approach based on the Liouville space formulation, but we use a different form than Dillon used for the O_2-O_2 short-range intermolecular potential and different parameters for the entire potential. Consideration is also given to the coupling between molecular states of different rotation quantum numbers.

JSEP

2. Line-Shape Expression

JSEP

Two approximations have been used in the calculation: (i) the impact approximation, which on the average entails only binary collisions at a particular instant, and leads to a linewidth expression proportional to pressure; and (ii) the classical path approximation, which implies that translational motions of molecules have no effect on their internal states. We believe that these approximations are justifiable for terrestrial atmospheric conditions.

The line-shape expression in the Liouville space formulation is given by

$$F(\omega) = -\frac{1}{\pi} \operatorname{Im} \sum_{\substack{j_a, j_\alpha \\ j_b, j_\beta}} \langle\langle j_a j_\alpha \| x \cdot x^* \| j_b j_\beta \rangle\rangle \langle\langle j_b j_\beta \| \frac{1}{\omega - \omega_o - n\langle m \rangle} \| j_a j_\alpha \rangle\rangle \langle j_a \| \rho \| j_\alpha \rangle, \qquad (1)$$

where $|j_a j_\alpha\rangle\rangle$ is a basis vector in line space, j_a, j_α being the molecular quantum states corresponding to a particular line; $\langle\langle j_a j_\alpha \| x \cdot x^* \| j_b j_\beta \rangle\rangle = \langle j_\alpha \| x \| j_a \rangle \langle j_b \| x^* \| j_\beta \rangle$ are the dipole moment matrix elements; ω_o is the resonance frequency corresponding to a particular line; ρ is the density matrix for the radiating molecules; and $n\langle m \rangle_{ij}$ is the thermal bath average of the interaction between lines i and j, where n is the number density of perturbing molecules.

The matrix elements $n\langle m \rangle_{ij}$ provide all crucial information on line broadening, the diagonal elements giving the linewidths and frequency shifts, and the off-diagonal elements accounting for the overlapping effects. In principle, we have

$$\langle m \rangle_{ij} = -i \langle v_o \langle\langle i \| 1 - S_\ell S_r^* \| j \rangle\rangle \rangle, \qquad (2)$$

where $S = \exp\left(\frac{1}{\hbar} \int_{-\infty}^{\infty} V \, dt\right)$ is the scattering operator which approaches 1 as the interaction potential $V \to 0$, and subscripts ℓ and r denote left and right operators in the Liouville formalism. If i represents the line $|j_a m_a; j_\alpha m_\alpha\rangle\rangle$ and j represents the line $|j_b m_b; j_\beta m_\beta\rangle\rangle$, where the m are magnetic quantum numbers, Eq. 2 written more fully becomes

$$i\left\langle \frac{m}{v_o} \right\rangle_{ij} = \delta_{ij} - \langle \langle\langle i \| S_\ell S_r^* \| j \rangle\rangle \rangle$$

$$= \delta_{ij} - \langle \langle\langle j_a m_a j_\alpha m_\alpha \| S_\ell S_r^* \| j_b m_b j_\beta m_\beta \rangle\rangle \rangle$$

$$= \delta_{ij} - \langle \langle j_a m_a | S | j_b m_b \rangle \langle j_\alpha m_\alpha | S | j_\beta m_\beta \rangle^* \rangle. \qquad (3)$$

JSEP

JSEP

In principle, $S = \exp(-i/\hbar \int V\, dt)$ and the matrix elements appearing in (3) will have to be calculated by using a many-body field-theoretic approach. The impact approximation allows us, however, to use a semiclassical approach in which $\int_{-\infty}^{\infty} V(t)\, dt$ is calculated entirely by classical mechanics.

3. Collision Integral I_c

The collision integral is the quantity $\int_{-\infty}^{\infty} dt\, V(t)$ appearing in the expression for S, where V is the interaction potential between radiator and perturber. We use for O_2-O_2 a three-body potential with perturber orientations averaged over angles, which was adopted by Mingelgrin:[12]

$$V(r,\theta) = \left(A\, e^{-ar} - \frac{C}{r^6}\right) + P_2(\cos\theta)\left[Aa_r\, e^{-ar} - \frac{Ca_a}{r^6}\right], \tag{4}$$

where the variables r and θ are as depicted in Fig. VIII-1.

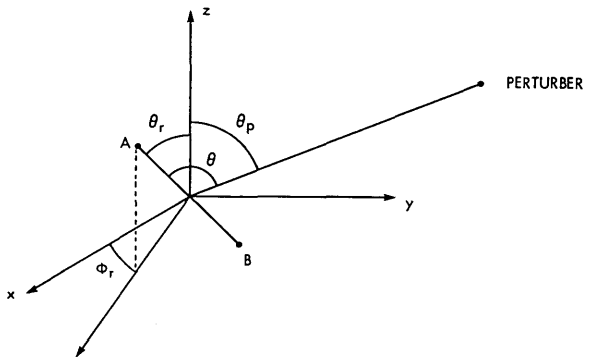

Fig. VIII-1. Geometrical configuration for radiator-perturber collision. Subscript r denotes radiator, subscript p denotes perturber; AB represents the radiator molecule; xyz is a set of space-fixed axes.

The constants in Eq. 4 have the numerical values[12]

$A = 1.503 \times 10^6$ eV

$C = 48.126$ eV $\mathring{A}^6$

$a = 5.258\ \mathring{A}^{-1}$

$a_r = 1.24$

JSEP

$a_a = 0.229$.

The time integration is converted to spatial integration by a change of variables $t \rightarrow r$. Thus

$$I_c = \int_{-\infty}^{\infty} V\, dt = \int V \frac{dt}{dr}\, dr = 2 \int_{r_o}^{\infty} dr \frac{V}{\dot{r}}, \tag{5}$$

where r_o is the distance of closest approach of the perturber. If we write

$$V(r, \theta) = V_1(r) + V_2(r)\, P_2(\cos\theta), \tag{6}$$

the collision integral I_c is finally reduced (see Fig. VIII-1) to the form

$$\begin{aligned} I_c &= \frac{8\pi}{5} \sum_m Y^*_{2,m}(\theta_r, \phi_r)\, Y^*_{2,m}(\theta_{p_o}, 0) \int_{r_o}^{\infty} dr \frac{V_2(r)}{\dot{r}} \\ &= 2P_2(\cos\psi) \int_{r_o}^{\infty} dr \frac{V_2(r)}{\dot{r}} \\ &= \hbar K_2 P_2(\cos\psi), \end{aligned} \tag{7}$$

where

$$K_2(b, v_o) = \frac{2}{\hbar}\left(\frac{\mu}{2}\right)^{1/2} \int_{r_o}^{\infty} dr \frac{Aa_r\, e^{-ar} - \frac{Ca_a}{r^6}}{\left\{\frac{1}{2}\mu v_o^2 \left(1 - \frac{b^2}{r^2}\right) - A\, e^{-ar} + \frac{C}{r^6}\right\}^{1/2}} \tag{8}$$

μ = reduced mass of the interacting system

v_o = initial velocity of the perturber

b = impact parameter

$\theta_{p_o} = \theta_p$ at closest approach configuration

$\psi = \theta$ at closest approach configuration

and $r_o(b, v_o)$ is obtained from the solution of the equation

$$\frac{1}{2}\mu v_o^2 \left(1 - \frac{b^2}{r_o^2}\right) - A\, e^{-ar_o} + \frac{C}{r_o^6} = 0. \tag{9}$$

In arriving at Eq. 7 the following points should be noted:

1. Only $V_1(r)$ is used in $\dot{r}$, that is, in the calculation of the translational motion;

JSEP

this procedure is a consequence of the classical path approximation.

2. $V_1(r)$, the angle-independent term in V, does not contribute to broadening, hence the absence of this term in the numerator of the integrand in Eq. 7, which is a consequence of Eq. 3.

3. In Eq. 7 the quantity $Y^*_{2m}(\theta_p(r), 0)$ should be part of the integrand. But the main contribution to the integral comes from near r_o at which $\frac{1}{\dot{r}} \to \infty$ and $Y_{2m}(\theta_p(r), 0)$ varies much more slowly than $\frac{1}{\dot{r}}$, hence it is taken outside the integral and treated as a constant.

The quantities $x_o(b, v_o)$ and $K_2(b, v_o)$ are calculated for a representative set of (b, v_o) for a particular temperature T. For T = 300°K, we have chosen 15 values of v_o for calculation:

$$(2, 3, 4, 5, 5.5, 6, 7, 8, 9, 10, 20, 30, 40, 50, 60) \times 10^4 \text{ cm/s}$$

and 51 values of b, from 0 Å to 10 Å at 0.2 Å intervals.

The values of v_o are chosen by consideration of the Boltzmann distribution and of b from the fact that K_2 rapidly approaches zero for $b > 10$ Å. Equation 9 for x_o is solved by an iterative algorithm and the K_2 are calculated by a 10-point Gaussian quadrature.

4. Interaction Matrix $\langle m \rangle_{ij}$

The operator $S = e^{-iK_2P_2}$ is expanded in the form

$$S = \sum_j \tau_j P_{2j}(\cos\psi)$$

$$= \sum_j \sum_m \frac{4\pi}{4j+1} \tau_j Y^*_{2j,m}(\theta_{p_o}, 0)\, Y_{2j,m}(\theta_r, \phi_r), \tag{10}$$

where the τ_j depend only on K_2 and only the quantity $Y_{2j,m}(\theta_r, \phi_r)$ connects the two states $|N_a, j_a, j_\alpha\rangle\rangle$ and $|N_b, j_b, j_\beta\rangle\rangle$ in a general matrix element, since only this quantity depends on the radiator angles. We can then show that

$$\langle\langle N_a, j_a, j_\alpha \| S_\ell S^*_r \| N_b, j_b, j_\beta \rangle\rangle$$

$$= \sum_{j_1} \sum_{j_2} \sum_j C_{j_1 j_2 j} \tau_{j_1} \tau^*_{j_2} P_{2j}(\theta_{p_o}), \tag{11}$$

JSEP

where

$$C_{j_1 j_2 j} = (-1)^{j_a + j_\beta} \left[(2j_a+1)(2j_b+1)(2j_\alpha+1)(2j_\beta+1)\right]^{1/2} (2N_a+1)(2N_b+1)$$

$$\times \begin{Bmatrix} N_a & j_a & 1 \\ j_b & N_b & 2j_1 \end{Bmatrix} \begin{pmatrix} N_a & 2j_1 & N_b \\ 0 & 0 & 0 \end{pmatrix} \begin{Bmatrix} N_a & j_\alpha & 1 \\ j_\beta & N_b & 2j_2 \end{Bmatrix} \begin{pmatrix} N_a & 2j_2 & N_b \\ 0 & 0 & 0 \end{pmatrix}$$

$$\times (4j+1) \begin{pmatrix} 2j_1 & 2j_2 & 2j \\ 0 & 0 & 0 \end{pmatrix} \sum_{m_\alpha} \sum_{m_\beta} \begin{pmatrix} j_\alpha & 2j_2 & j_\beta \\ -m_\alpha & m_\alpha - m_\beta & m_\beta \end{pmatrix} \begin{pmatrix} 2j_1 & 2j_2 & 2j \\ m_\beta - m_\alpha & m_\alpha - m_\beta & 0 \end{pmatrix}$$

$$\left[\begin{pmatrix} j_a & 1 & j_\alpha \\ -m_\alpha & 0 & m_\alpha \end{pmatrix} \begin{pmatrix} j_b & 1 & j_\beta \\ -m_\beta & 0 & m_\beta \end{pmatrix} \begin{pmatrix} j_a & 2j_1 & j_b \\ -m_\alpha & m_\alpha - m_\beta & m_\beta \end{pmatrix} \right.$$

$$\left. - 2 \begin{pmatrix} j_a & 1 & j_\alpha \\ -(m_\alpha+1) & 1 & m_\alpha \end{pmatrix} \begin{pmatrix} j_b & 1 & j_\beta \\ -(m_\beta+1) & 1 & m_\beta \end{pmatrix} \begin{pmatrix} j_a & 2j_1 & j_b \\ -(1+m_\alpha) & m_\alpha - m_\beta & m_\beta + 1 \end{pmatrix} \right]. \qquad (12)$$

In the summations in Eqs. 11 and 12 the ranges of the indices j_1, j_2, j, m_α, and m_β are limited by the 3j and 6j symbols, that is, by the angular momentum quantum numbers $N_a, j_a, j_\alpha, N_b, j_b, j_\beta$.

A general element of the interaction matrix may then be written

$$i\, n\langle m \rangle_{\mu\nu} = n \left\langle v_o \delta_{\mu\nu} - v_o \sum_{j_1 j_2 j} C_{j_1 j_2 j} \tau_{j_1} \tau^*_{j_2} P_{2j}(\theta_{p_o}) \right\rangle$$

$$= \frac{2\pi P}{kT} \int_0^\infty dv_o\, M(v_o)\, v_o \left[\delta_{\mu\nu} \int_0^{b'} db\, b - \sum_{j_1 j_2 j} C_{j_1 j_2 j} \int_0^{b'} db\, b \tau_{j_1} \tau^*_{j_2} P_{2j} \right], \qquad (13)$$

where μ, ν denote the two lines, $M(v_o)$ the Boltzmann velocity distribution function; P is pressure; k, Boltzmann's constant; T, temperature (°K); b', upper limit of impact parameter of perturbers above which no significant interaction between molecules occurs (b' is taken as 10 Å in the present set of calculations). Note that to express $n\langle m \rangle_{\mu\nu}$ in hertzian units Eq. 24 must be divided by 2π. For the case of oxygen, for each rotational quantum number N, there are 6 basis line states $|N_a, j_a, j_\alpha\rangle\rangle$:

$|N, N, N+1\rangle\rangle$

$|N, N+1, N\rangle\rangle$

$|N, N, N-1\rangle\rangle$

JSEP

$|N, N-1, N\rangle\rangle$

$|N, N+1, N+1\rangle\rangle$

$|N, N-1, N-1\rangle\rangle$

representing the $N \rightarrow N+1$, $N \rightarrow N-1$ transitions, their corresponding negative resonance branches, and nonresonant absorption. Note that Eqs. 11, 12, and 13 provide a means of calculating the interaction between any two lines, even lines belonging to different N. Note also that the matrix $n\langle m\rangle_{\mu\nu}$ is symmetrical.

5. Results: Linewidths and Absorption Coefficients

In taking the Boltzmann average as indicated in Eq. 13, the quantity to be averaged is fitted first to a polynomial as a function of v_o so that the integration can be carried out analytically. Figure VIII-2 and the numerical values in Table VIII-1 show results of a

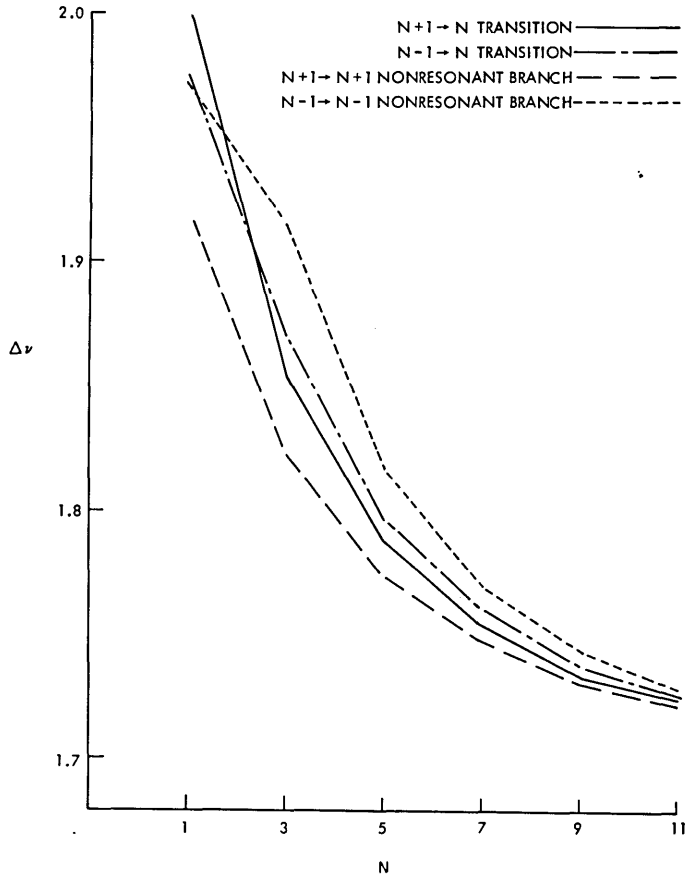

Fig. VIII-2. Linewidths (MHz/Torr) for oxygen lines arising from rotation quantum number N = 1, 3, 5, 7, 9, 11 at T = 300°K. Only O_2-O_2 collision effects are considered.

JSEP

Table VIII-1. Absorption coefficients for O_2 as a function of frequency at P = 760 Torr and T = 300°K for 4 cases of matrix element configurations. Only lines arising from rotation quantum number N = 1, 3, 5, 7, 9, 11 and O_2-O_2 collisions are considered.

JSEP

ν (GHz)	K_ν (Np/km)			
	1	2	3	4
50	0.45830×10^{-1}	0.41390×10^{-1}	0.39881×10^{-1}	0.39493×10^{-1}
51	0.59570×10^{-1}	0.53843×10^{-1}	0.51898×10^{-1}	0.51398×10^{-1}
52	0.80226×10^{-1}	0.72633×10^{-1}	0.70061×10^{-1}	0.69401×10^{-1}
53	0.11338	0.10297	0.99450×10^{-1}	0.98551×10^{-1}
54	0.17159	0.15671	0.15171	0.15045
55	0.28601	0.26384	0.25645	0.25464
56	0.52707	0.49378	0.48284	0.48041
57	1.0582	1.0176	1.0033	1.0005
58	2.0540	2.0950	2.0985	2.0995
59	2.5991	2.7258	2.7708	2.7810
60	2.7977	2.9467	3.0152	3.0307
61	2.7156	2.8639	2.9101	2.9212
62	1.8631	1.8367	1.8246	1.8233
63	0.97673	0.92164	0.90278	0.89862
64	0.51277	0.47258	0.45862	0.45520
65	0.30698	0.27892	0.26911	0.26664
66	0.20680	0.18628	0.17909	0.17727
67	0.15095	0.13522	0.12971	0.12831
68	0.11643	0.10390	0.99517×10^{-1}	0.98405×10^{-1}
69	0.93452×10^{-1}	0.83166×10^{-1}	0.79565×10^{-1}	0.78654×10^{-1}
70	0.77286×10^{-1}	0.68636×10^{-1}	0.65609×10^{-1}	0.64844×10^{-1}

JSEP

JSEP

ninth-degree polynomial fitting.

The absorption coefficient for O_2 is given by

$$K_\nu = 0.61576 \frac{P\nu^2}{T^3} (-1) \operatorname{Im} \left\{ \underline{d} \cdot \frac{1}{\underline{\underline{\nu}} - \underline{\underline{\nu}}_o - \frac{n\langle \underline{\underline{m}} \rangle}{2\pi}} \cdot \underline{\underline{\rho}}' \cdot \underline{d} \right\}, \tag{14}$$

where P is in Torr, ν in GHz, and T in °K; $\underline{\underline{\rho}}'$ is the population matrix excluding the partition function; and $\underline{d}$ is the dipole moment matrix. The matrix to be inverted is

$$\underline{\underline{\nu}} - \underline{\underline{\nu}}_o - \frac{1}{2\pi} n\langle \underline{\underline{m}} \rangle = \underline{\underline{\nu}} - \underline{\underline{\nu}}_o + iP\underline{\underline{M}},$$

where

$$M = \frac{in}{2\pi P} \langle \underline{\underline{m}} \rangle. \tag{15}$$

In order to avoid doing an inversion process for each observation frequency ν, we adopt the following procedure: Diagonalize $-\underline{\underline{\nu}}_o + iP\underline{\underline{M}}$ so that

$$\underline{\underline{\lambda}}(\text{diagonal}) = \underline{\underline{A}}^{-1} \cdot (-\underline{\underline{\nu}}_o + iP\underline{\underline{M}}) \cdot \underline{\underline{A}}. \tag{16}$$

Then

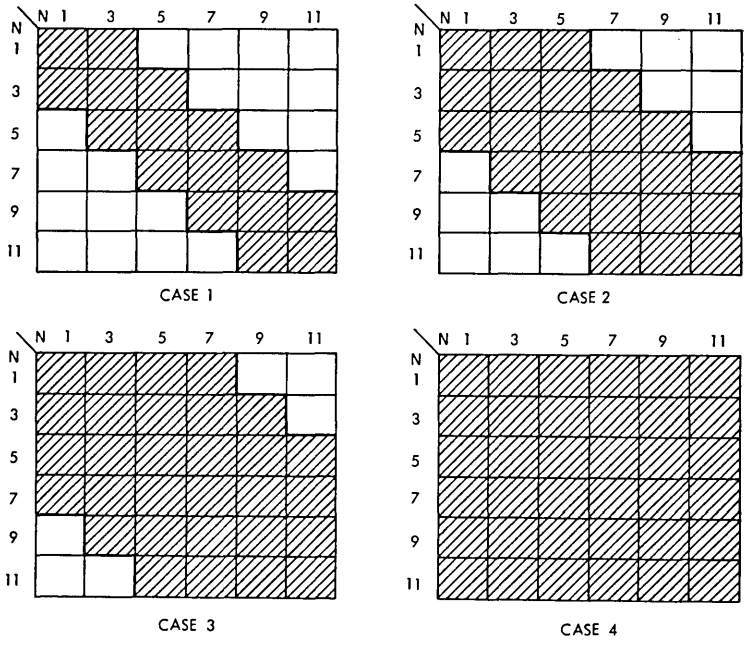

Fig. VIII-3. Comparison of the off-diagonal elements of the interaction matrix for 4 cases. Each square block represents a 6 × 6 matrix. All matrix elements outside of shaded areas are taken to be zero.

JSEP

$$(\nu\underline{\underline{I}} - \underline{\underline{\nu}}_o + iP\underline{\underline{M}})^{-1} = \underline{\underline{A}} \cdot (\nu\underline{\underline{I}} + \underline{\underline{\lambda}})^{-1} \cdot \underline{\underline{A}}^{-1} \tag{17}$$

JSEP

and we have

$$K_\nu = 0.61576 \frac{P\nu^2}{T^3} (-1)\mathrm{Im}\left[\underline{d} \cdot \underline{\underline{A}} \cdot (\nu\underline{\underline{I}} + \underline{\underline{\lambda}})^{-1} \cdot \underline{\underline{A}}^{-1} \cdot \underline{\underline{\rho}}' \cdot \underline{d}\right]. \tag{18}$$

The matrix $\underline{\underline{M}}$ is 66×66 for taking lines up to N = 11. To investigate the relative contributions of off-diagonal elements of the interaction matrix, we compared the K_ν for 4 cases in Fig. VIII-3.

Results from Table VIII-1 indicate that Case 3 is a close approximation to Case 4. If by $\mathscr{E}_{ij}(\nu)$ we denote the relative error between case i and case j at frequency ν, it can be seen that $\mathscr{E}_{14}(60) \sim 7.7\%$, $\mathscr{E}_{24}(60) \sim 6.1\%$, $\mathscr{E}_{34}(60) \sim 0.5\%$; $\mathscr{E}_{14}(50) \sim 16\%$, $\mathscr{E}_{24}(50) \sim 4.9\%$, $\mathscr{E}_{34}(50) \sim 0.9\%$. This suggests that in future computations, when the matrix is to be enlarged, only the Case 3 configuration need be used. Thus by equating most of the matrix elements to zero, a great saving of labor can be accomplished in computations.

References

1. J. H. Van Vleck and V. F. Weisskopf, Rev. Mod. Phys. 17, 227 (1945).
2. E. P. Gross, Phys. Rev. 97, 395 (1955).
3. P. W. Anderson, Phys. Rev. 76, 647 (1949).
4. M. Baranger, Phys. Rev. 111, 481 (1958); 111, 494 (1958); 112, 855 (1958).
5. U. Fano, Phys. Rev. 131, 259 (1963).
6. A. Ben-Reuven, Phys. Rev. 145, 7 (1966).
7. R. G. Gordon, J. Chem. Phys. 46, 448 (1967).
8. J. Gersten and H. M. Foley, Phys. Rev. 182, 24 (1969).
9. T. A. Dillon, E. W. Smith, and J. Cooper, Phys. Rev. A 2, 1839 (1970); T. A. Dillon and J. T. Godfrey, Phys. Rev. A 5, 599 (1972).
10. D. W. Ross, Ann. Phys. (N.Y.) 36, 458 (1966).
11. B. Bezzerides, J. Quant. Spectrosc. Radiat. Transfer 7, 353 (1967); Phys. Rev. 181, 379 (1969).
12. U. Mingelgrin, Ph.D. Dissertation, Harvard University, 1972.

JSEP

B. ATMOSPHERIC MILLIMETER-WAVE OPACITY DUE TO OXYGEN AND WATER VAPOR

National Aeronautics and Space Administration (Contract NAS1-10693)

Philip W. Rosenkranz

The opacity of the U.S. Standard Atmosphere has been computed using a model for absorption by molecular oxygen based on overlapping-line theory.[1] It is well known that the opacity of the wings of the oxygen band is less than is predicted by a summation of individual lines, with overlap effects not considered. The explanation for this phenomenon is that the interference of the lines subtracts from the resonant (Lorentzian) contribution in the wings, thereby making the band narrower (see Sec. VIII-A). Another interesting matter is that above 160 GHz, the computed opacity is less than the nonresonant contribution (which is 0.03 dB above ~1 GHz). This is also an interference effect caused by the merging (collapse) of the entire fine-structure spectrum. These computations are illustrated by Fig. VIII-4.

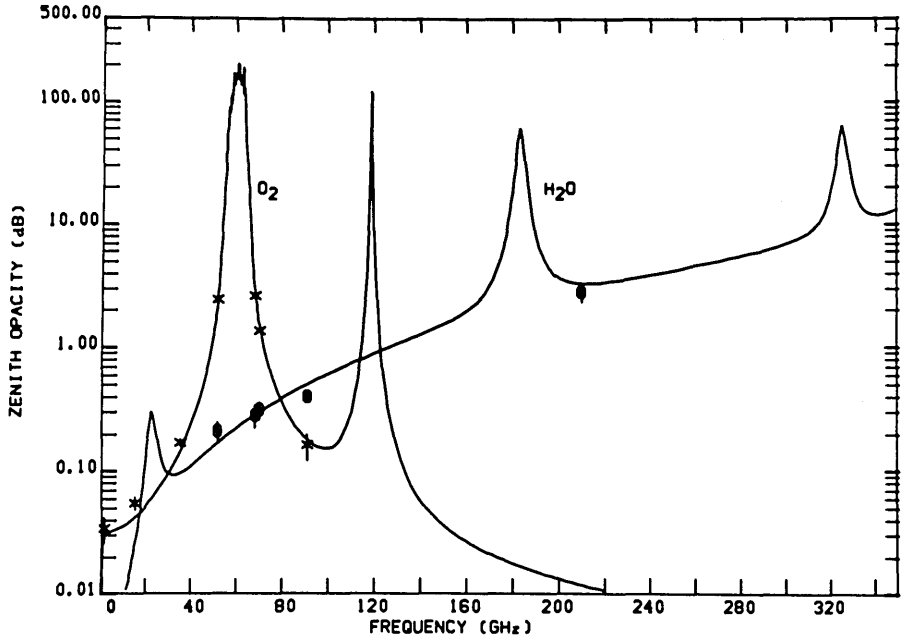

Fig. VIII-4. Sea-level zenith opacity in the U.S. Standard Atmosphere for oxygen and 1 precipitable cm water vapor with a scale height of 2 km. Measurements for oxygen (×) and water vapor (⊕) are from refs. 7-11.

Isolated spectral lines such as those of water vapor have been interpreted traditionally by using the theories of Van Vleck and Weisskopf[2] or of Gross.[3] Becker and Autler[4] found that the Van Vleck-Weisskopf line shape fits the 22.235 GHz water-vapor line

very well, when a continuum absorption proportional to the frequency squared was added. The Gross line shape fits less well.[5]

Both Van Vleck-Weisskopf and Gross line shapes may be derived as special cases from overlapping-line theory. The former results when there is no interference; the latter when each line couples only to its conjugate resonance at negative frequency. The fact that the Van Vleck-Weisskopf line shape fits the 22 GHz line implies either that interference cancels or is negligible for this line. This conclusion cannot be generalized to the other lines a priori, but for the purpose of computation in Fig. VIII-4 we have used the Van Vleck-Weisskopf shape for all of the water-vapor lines.

The continuum absorption of water vapor was computed by summing the 25 lowest lines and adding a term that is adjusted slightly from that of Gaut and Reifenstein:[6]

$$\gamma_{excess} = 5.3 \cdot 10^{-9}\, \rho P \nu^2 \left(\frac{300}{T}\right)^{2.1},$$

where γ is absorption in dB/km, ρ is water-vapor density in g/m^3, P is total pressure in mb, ν is frequency in GHz, and T is temperature in °K. This is an empirical correction that appears to hold up at least to 1000 GHz, but for which at present there is no completely satisfactory explanation.

References

1. P. W. Rosenkranz, "Shape of the 5-mm Oxygen Band in the Atmosphere," IEEE Trans. on Antennas and Propagation, in press.
2. J. H. Van Vleck and V. F. Weisskopf, Rev. Mod. Phys. 17, 227 (1945).
3. E. P. Gross, Phys. Rev. 97, 395 (1955).
4. G. E. Becker and S. H. Autler, Phys. Rev. 70, 300 (1946).
5. P. W. Rosenkranz, a paper to be presented at the Optical Society of America Topical Meeting on Remote Sensing of the Atmosphere, Anaheim, California, March 1975.
6. N. E. Gaut and E. C. Reifenstein, "Interaction Model of Microwave Energy and Atmospheric Variables," Technical Report 13, Environmental Research and Technology, Inc., Lexington, Massachusetts, February 26, 1971.
7. T. F. Howell and J. R. Shakeshaft, J. Atmospheric and Terrest. Phys. 29, 1559 (1967).
8. E. E. Altshuler, V. J. Falcone, and K. N. Wulfsberg, IEEE Spectrum 5 (7), 83 (1968).
9. E. E. Reber, J. Geophys. Res. 77, 3831 (1972).
10. F. I. Shimabukuro and E. E. Epstein, IEEE Trans., Vol. AP-18, No. 4, p. 485, July 1970.
11. W. A. Johnson, T. T. Mori, and F. I. Shimabukuro, IEEE Trans., Vol. AP-18, No. 4, p. 512, July 1970.